JOURNAL OF PROPULSION AND POWER
Vol. 27, No. 1, January–February 2011

Inferencing Component Maps of Gas Turbine Engine Using Bayesian Framework

Piyush M. Tagade* and K. Sudhakar†
Indian Institute of Technology, Mumbai 400 076, India

DOI: 10.2514/1.47329

A Bayesian framework is proposed for characterization of uncertainty in gas turbine performance predictions induced by poorly known component maps and uncertain model structure. Uncertainty in component maps and the model structure is characterized by independent Gaussian processes. Bayesian calibration is used to update the uncertainty whenever new information is available through experimental observations and expert opinion. The Markov Chain Monte–Carlo method is used to sample from posterior distribution. Parameters from the posterior distribution are identified that provide information about the validity of the model and experimental observations. Updated uncertainty is propagated to system response using the Monte–Carlo method. The propagated uncertainty in system response is represented using Bayesian confidence bounds. Proposed framework is demonstrated for calibration of a design intent single spool turbojet engine simulator. Compressor and turbine maps are inferred using the Bayesian framework.

Nomenclature

CN	=	corrected speed
f	=	probability density function
I	=	polar moment of inertia, kg · m^2
N	=	spool speed, rev/s
P	=	pressure, Pa
Pr	=	probability
R	=	gas constant
T	=	simulator
V	=	lumped volume, m^3
W	=	mass flow rate, kg/s
$\bar{x}$	=	vector of control input
Y	=	system response
γ	=	isentropic index
δ	=	discrepancy function
ε	=	measurement uncertainty
ζ	=	true system response
$\bar{\eta}$	=	component maps
λ	=	hyperparameters of the Gaussian process
μ	=	mean
Σ	=	covariance matrix
σ	=	standard deviation
τ	=	torque, N · m
$\bar{\Psi}$	=	state vector

Subscripts

3	=	compressor exit
5	=	turbine exit
C	=	compressor
e	=	experiment
F	=	fuel
J	=	jet pipe
NZ	=	nozzle
S	=	scaling
T	=	turbine
t	=	true
U	=	upstream

Received 14 January 2010; revision received 25 June 2010; accepted for publication 23 September 2010.

*Research Scholar, Department of Aerospace Engineering, I.I.T., Bombay, Powai.

†Professor, Department of Aerospace Engineering, I.I.T., Bombay, Powai.

Introduction

WITH present advancements in the digital technologies, computer simulators have become a preferred source of knowledge acquisition. Often experimental observations and expert opinion are used as auxiliary sources of information, especially to calibrate, validate and determine parameters of a simulator. Researchers have identified varied sources of uncertainties in computer simulators [1], experimental observations [2], and expert opinion [3]. These uncertainties induce uncertainty in simulator predictions that may significantly impact decisions based on the predictions. To analyze risk associated with the decisions, it is necessary to quantify uncertainty in the simulator predictions. Researchers have already stressed upon a need for a framework to identify, elicit, and characterize uncertainties in computer simulators [4–6]. The framework is expected to provide a methodology to update uncertainty in a simulator whenever new information is available through experimental observations and expert opinion. The framework should also provide methodologies for propagation of uncertainty to simulator predictions.

Simulator is a digital representation of mathematical model that is derived using physics-based theory. Simulator predicts system response on specification of control inputs and parameters. The parameters can be classified as physics-based or tuning parameters which are unique for a particular simulator. Physics-based parameters are uncertain due to experimental uncertainties, whereas tuning parameters are uncertain by definition itself. Simulator model are often uncertain owing to unknown physics, availability of multiple theories, various approximations, and unconfirmed veracity and validity of the model. Such uncertainty is termed as model structure uncertainty. The uncertainty is classified as aleatory and epistemic uncertainty. Aleatory uncertainty is defined as an uncertainty due to inherent variability in the system, whereas epistemic uncertainty emanates due to lack of knowledge. Different types of uncertainty require different mathematical representation. Aleatory uncertainty is always represented using probability theory, whereas for epistemic uncertainty, probabilistic [7] as well as various nonprobabilistic [8] representations are proposed in the literature.

In the present paper, Bayesian probability theory is used to represent both aleatory and epistemic uncertainty. It may be noted that the domain of applicability of Bayesian probability theory forms a subset of domain of applicability of nonprobabilistic methods. Bayesian probability measure approximates nonprobabilistic measure to arbitrary accuracy on the subset. Since the subset covers

domain of interest of the present investigation, use of Bayesian probability theory suffices. See de Finetti [9], Bernardo and Smith [10] and Robert [11] for details of the Bayesian probability theory. The framework where Bayesian probability theory is used to characterize uncertainty is termed as Bayesian framework. In the framework, Bayesian calibration method is used to update uncertainty in the simulator whenever new information is available. The uncertainty conditional on the added new information is propagated to the simulator predictions using uncertainty propagation methods like Monte Carlo, moment methods, and polynomial chaos method. See Glimm and Sharp [12] for earlier applications of Bayesian framework. Present state of the art in the field is based on the seminal work by Kennedy and O'Hagan [13], where Bayesian framework is proposed for calibration of a computer simulator. In that paper, uncertainty in parameters, model structural uncertainty and the uncertainty due to limited number of available simulation runs is considered. See Higdon et al. [14], Goldstein and Rougier [15] and Paulo et al. [16] for application of the methodology to problems of engineering interest. See Trucano et al. [17] and Kelly and Smith [18] for an extensive review of the research work in this field.

The research presented in this paper is motivated by need to quantify uncertainty in performance predictions of a gas turbine engine. Gas turbine engine simulators used during initial design stage are predominantly based on low-fidelity models, with most of the components described using performance maps. For an engine with a novel design concept, or during engine design by an organization without prior expertise, component performance maps are unknown or poorly known initially, introducing uncertainty in component maps. Further, model structure is also uncertain owing to the use of low-fidelity models. Uncertainty in component maps and model structure induces uncertainty in simulator predictions. Knowledge of the uncertainty in simulator predictions is expected to help immensely in various design decisions, especially during control system design. However, there is a dearth of research efforts in the field of uncertainty characterization and calibration of a gas turbine engine simulator in presence of uncertainty, with notable exception of the efforts by Roth et al. [19,20] and Doel et al. [21]. Application of full Bayesian framework for a gas turbine engine simulation is not yet reported in the literature.

In the present paper, efficacy of the Bayesian framework is demonstrated for calibration of a single spool gas turbine engine simulator. Calibration of a gas turbine simulator requires probabilistic representation of component maps. Component map is a function that provides required performance value of component on specification of appropriate inputs. Representation of uncertainty in a component map requires specification of probability distribution on a set of all such possible functions that forms a noncountably infinite dimensional functional space. However, present state of the art in the field of Bayesian calibration is limited for calibration of simulators with finite dimensional parameter space [13].

Tagade et al. [22] have proposed use of nonstationary Gaussian process for probabilistic representation of component maps. Tagade et al. [22] have demonstrated efficacy of the Bayesian framework for inference of compressor map. They propose a two step approach to ensure robustness with respect to the prior. Proposed method admits information from experimental observations and expert judgment to infer component maps. The methodology is demonstrated using hypothetical test bed data for calibration of a single spool turbojet engine simulator with uncertainty in compressor map. Tagade et al. [22] have used the framework for calibration of a perfect simulator where uncertainty in the model is absent. However as already identified, simulator models are always expected to be structurally uncertain. If effect of the model structure uncertainty is not considered, calibration attributes discrepancy in the model to the component maps. Thus, uncertainty in the model significantly affects, and often limits, capability to calibrate the simulator. In the present paper, methodology proposed by Tagade et al. [22] is extended to take into consideration effect of uncertainty in the model structure. Uncertainty in both compressor and turbine map is considered. The methodology is demonstrated for calibration of a single spool turbojet engine simulator using test bed data of a design intent engine.

The rest of the paper is organized as follows. Section 2 provides statistical formulation of the problem. In Sec. 3, gas turbine engine model is discussed. Detailed discussion of the Bayesian framework is provided in Sec. 4. In Sec. 5, details of implementation of the framework are provided. In Sec. 6 results are reported and finally in Sec. 7, the paper is summarized and concluded.

Statistical Formulation

A gas turbine engine is studied at a given control input setting $\bar{x}$. Typically M different system responses are investigated at any $\bar{x}$. Let $\zeta_j(\bar{x})$ denote jth true system response that represents true but unknown behavior of the engine. Engine is experimentally observed on the test bed to determine the value of $\zeta_j(\bar{x})$. Let $y_{e_j}(\bar{x})$ denote experimental observation of the jth system response. However, experimental observations are always uncertain, limiting the accuracy to which $\zeta_j(\bar{x})$ can be known. Let $\varepsilon_j(\bar{x})$ denote experimental uncertainty in jth observed system response. The relationship between true system response and observed system response is given by

$$y_{e_j}(\bar{x}) = \zeta_j(\bar{x}) + \varepsilon_j(\bar{x}) \tag{1}$$

The present paper treats expert opinion similar to experimental observations with quantified uncertainty. The following discussion may be applied for expert opinion without any change.

A computer simulator based on a mathematical model is used to predict system response of a gas turbine engine. The model is a function T_j that maps control input $\bar{x}$ to engine system response on specification of component maps. A component map η is a function that maps arguments $\bar{\chi}$ that are defined at control inputs $\bar{x}$ to the required performance value. Values of arguments $\bar{\chi}$ are realized by intermediate calculations of the simulator model. Let $\bar{\eta}$ denote a set of uncertain component maps required by the simulator while $\bar{\eta}_t$ denote the set of true but unknown performance maps. Because of uncertainty in the model, simulation predictions deviate from the true system response even if true component maps are available. On specification of true component maps, difference between jth true system response and model prediction is given by a function $\delta_j(\bar{x})$, termed here as discrepancy function. Thus, relationship between simulator prediction and the true system response is given by

$$\zeta_j(\bar{x}) = T_j(\bar{x}, \bar{\eta}_t) + \delta_j(\bar{x}) \tag{2}$$

It may be noted that the discrepancy function is also defined at true component maps. Using Eqs. (1) and (2), the relationship between experimental observation and simulator prediction is given by

$$y_{e_j}(\bar{x}) = T_j(\bar{x}, \bar{\eta}_t) + \delta_j(\bar{x}) + \varepsilon_j(\bar{x}) \tag{3}$$

where $\bar{\eta}_t$, $\delta_j(\bar{x})$, and $\varepsilon_j(\bar{x})$ are uncertain. Because experimental observations are expected to be available with quantified uncertainty, probability distribution of $\varepsilon_j(\bar{x})$ is known. On specification of $y_{e_j}(\bar{x})$, Bayes theorem is used to update uncertainty in $\bar{\eta}_t$ and $\delta_j(\bar{x})$. Bayes theorem provides update of the prior knowledge of an uncertain variable whenever new information is available. Equation (3) and Bayes theorem gives

$$f(\bar{\eta}_t, \delta_j(\bar{x}) | y_{e_j}(\bar{x})) \propto \Pr(y_{e_j}(\bar{x}) | T_j(\bar{x}, \bar{\eta}_t), \delta_j(\bar{x})) \times f(\bar{\eta}_t, \delta_j(\bar{x})) \tag{4}$$

where $f(\bar{\eta}_t, \delta_j(\bar{x}))$ is known as prior, $\Pr(y_{e_j}(\bar{x}) | T_j(\bar{x}, \bar{\eta}_t), \delta_j(\bar{x}))$ is known as likelihood and $f(\bar{\eta}_t, \delta_j(\bar{x}) | y_{e_j}(\bar{x}))$ is known as posterior probability.

Often, gas turbine engine is investigated at N different control input settings. Let us define a vector of N experimental observations of jth system response as

$$\bar{Y}_{e_j} = \{y_{e_j}(\bar{x}_i)\}; \qquad i = 1, \ldots, N \tag{5}$$

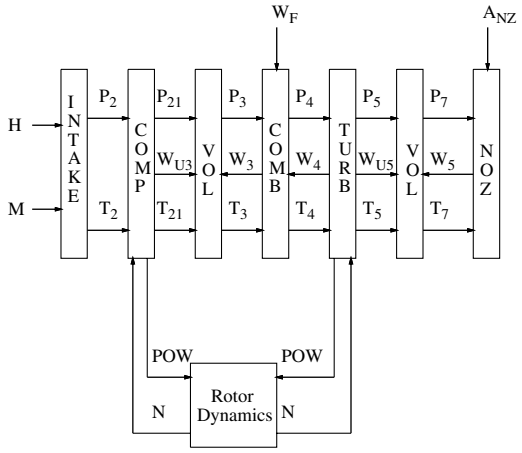

Fig. 1 Single spool turbojet engine model.

and a vector of experimental observations of all such system responses is

$$\bar{Y}_e = \{\bar{Y}_{e_j}\}; \qquad j = 1, \ldots, M \tag{6}$$

For the same system response, define a vector $\bar{d}_j$ as

$$\bar{d}_j = \{T_j(\bar{x}_i, \bar{\eta}_t) + \delta_j(\bar{x}_i)\}; \qquad i = 1, \ldots, N \tag{7}$$

and a vector $\bar{d}$ as

$$\bar{d} = \{\bar{d}_j\}; \qquad j = 1, \ldots, M \tag{8}$$

For notational convenience, let us also define a set

$$\bar{\delta}_j = \{\delta_j(\bar{x}_i)\}; \qquad i = 1, \ldots, N \tag{9}$$

and

$$\bar{\delta} = \{\bar{\delta}_j\}, \qquad j = 1, \ldots, M \tag{10}$$

All the information available through experimental observations is used simultaneously to update uncertainty in component maps and model structure. Thus, Bayes theorem for Bayesian calibration of a gas turbine engine simulator is given by

$$f(\bar{\eta}_t, \bar{\delta}|\bar{Y}_e) \propto \Pr(\bar{Y}_e|\bar{d}) \times f(\bar{\eta}_t, \bar{\delta}) \tag{11}$$

The Bayesian calibration requires specification of prior probability distribution $f(\bar{\eta}_t, \bar{\delta})$ and likelihood $\Pr(\bar{Y}_e|\bar{d})$ that depends on simulator model $T(\bar{x}, \bar{\eta}_t)$. The following two sections provide detailed discussion of simulator model and specification of prior.

Gas Turbine Engine Model

Figure 1 shows schematic of the engine for which the Bayesian framework is investigated. The engine simulator model is based on a lumped volume approach [23], with static elements defined using aerothermodynamic relations and steady-state component maps. Difference between compressor and turbine torque results in change of spool speed, which is given by

$$\dot{N} = \frac{\tau_T - \tau_C}{2\pi I} \tag{12}$$

Lumped volume approach assumes accumulation of mass results in change in the total pressure. Thus pressure dynamics is given by

$$\dot{P} = \frac{\gamma RT}{V}(W_U - W) \tag{13}$$

where W_U is mass flow entering, while W is the mass flow exiting the lumped volume. Compressor and turbine are modeled using performance maps while other components are modeled using aerothermodynamic or empirical relations. The engine model is a set of three ordinary differential equations that predicts system response on specification of control inputs and component maps. For the present simulator, fuel flow rate W_F and nozzle throat area A_{NZ} are control inputs. Table 1 provide details of the engine model. Although demonstrated for a particular model, proposed Bayesian framework can be implemented for any simulator model without change in the methodology. Numerical integration techniques like Euler explicit or Newton Raphson method can be used to simulate the engine. Engine manufacturer specified lack of confidence in available compressor and turbine maps. Compressor map consist of mass flow rate map η_W^C and temperature ratio map η_{TR}^C while turbine map consist of mass flow rate map η_W^T and enthalpy rise map η_H^T. Bayesian framework is used to infer these maps.

Bayesian Framework

Two Step Approach

The framework requires specification of base component maps $\bar{\eta}_b$ to initiate the methodology. Tagade et al. [22] have proposed a two step approach for calibration that provide robustness with respect to choice of base component maps. In the first step, component maps are scaled using design point performance values that are inferred using Bayesian calibration. A single experimental observation, preferably at design point $\bar{x}_d$, is used. Uncertainty in the model is given by a random variable, which is a deviation function defined at a design point. In the second step, component maps are probabilistically represented using nonstationary Gaussian processes, while, deviation functions are modeled using stationary Gaussian processes.

Step One: Scaling Parameters

For compressor map, design point mass flow rate W_{Cd}^b and temperature ratio TR_{Cd}^b of the base map are used as scaling parameters. For turbine map design point mass flow rate W_{Td}^b and enthalpy rise H_{Td}^b are used as scaling parameters. Using scaling parameters, minimum performance value of base map is scaled to 0 while design point performance value is scaled to 1. On specification of arbitrary design point performance values, new maps can be obtained from the scaled base map using appropriate reverse scaling. See Tagade et al. [22] for further details. It may be noted that the methodology can be implemented without any change when efficiency is specified instead of temperature ratio or enthalpy rise. Uncertainty in component maps is specified by probability distribution on scaling parameters. Gaussian distribution with mean given by design point performance values of base map is used to specify prior on the scaling parameters. To approximate initial lack of knowledge about true component maps, high standard deviation is specified. Uncertainty in experimental observation is specified using zero-mean Gaussian distribution with standard deviation σ_{Y_j} for jth system response.

Difference between true and predicted jth system response is given by discrepancy function $\delta_j(\bar{x})$. Since a single experimental

Table 1 Engine model third-order ordinary differential equations

State variable	Description	Differential equation
N	Spool speed	$\dot{N} = (\frac{\tau_T - \tau_C}{2.0 \times \pi \times I})$
P_3	Total pressure at compressor exit	$\dot{P}_3 = (\frac{\gamma \times R \times \Upsilon_3}{V}) \times (W_{U3} - W_3)$
P_5	Total pressure at turbine exit	$\dot{P}_5 = (\frac{\gamma \times R \times \Upsilon_5}{V}) \times (W_{U5} - W_5)$

observation is used in step one, $\delta_j(\bar{x})$ is treated as a univariate random variable. Uncertainty in the model is given by probability distribution on this random variable. The first step assumes very high prior uncertainty in component maps, whereas, uncertainty in the model structure is comparatively low. Experimental observations are expected to provide more information about component maps as compared with the model structure uncertainty. Also, step one is mainly proposed to provide component maps for initiation of step two. Hence, uncertainty in $\delta_j(\bar{x})$ is specified using a known probability distribution and is not updated using Bayesian calibration. In the present paper, uncertainty in $\delta_j(\bar{x})$ is probabilistically represented using zero-mean Gaussian distribution with known standard deviation σ_{δ_j}. This probabilistic representation ensures that uncertainty in the model structure is not attributed to the uncertainty in component maps. Thus, the posterior probability is given by

$$f(\bar{\eta}_t|\bar{Y}_e,\bar{\delta}) \propto \prod_{j=1}^{M} \exp\left(-\frac{(y_{e_j}(\bar{x}_d)-T_j(\bar{x}_d,\bar{\eta}_t))^2}{2(\sigma^2_{\bar{Y}_{e_j}}+\sigma^2_{\delta_j})}\right) \times \exp\left(-\frac{(W_{Cd}-W^b_{Cd})^2}{2\sigma^2_{W_{Cd}}}\right) \times \exp\left(-\frac{(\mathrm{TR}_{Cd}-\mathrm{TR}^b_{Cd})^2}{2\sigma^2_{\mathrm{TR}_{Cd}}}\right) \times \exp\left(-\frac{(W_{Td}-W^b_{Td})^2}{2\sigma^2_{W_{Td}}}\right) \times \exp\left(-\frac{(H_{Td}-H^b_{Td})^2}{2\sigma^2_{H_{Td}}}\right) \quad (14)$$

Component maps calculated using mean of the posterior as scaling parameters are inferred maps after step one.

Step Two: Gaussian Process Representation

In the second step, component maps $\bar{\eta}_t$ and deviation function $\delta_j(\bar{x})$ are treated as random functions [24]. Gaussian process is used to specify uncertainty in random functions. Bayesian calibration is used to update these Gaussian processes. In the remainder of this section, details of the second step are provided.

Specification of Prior

A Gaussian process is completely defined on specification of mean and covariance function. Often, mean and covariance functions are defined using additional parameters, known as hyperparameters. Probability of a Gaussian process is given by a multivariate Gaussian distribution with mean and covariance function specified at finite locations. For component maps, nonstationary Gaussian process with mean function given by inferred map from step one is used. Stationary Gaussian process with uncertain hyperparameters is used to probabilistically represent deviation function. Hyper-parameters of the Gaussian process are inferred using Bayesian calibration.

Prior for Compressor Map

Compressor map is a specification of mass flow rate and temperature ratio as a function of pressure ratio and corrected speed. Usually, the function is specified by a finite set of values of mass flow rate and temperature ratio at discrete pressure ratio and corrected speed with associated interpolation. Let $\overline{\mathrm{PR}}_C = \{\mathrm{PR}^C_i\}$ denote a set of discrete pressure ratio and $\overline{\mathrm{CN}}_C = \{\mathrm{CN}^C_j\}$ be the set of discrete corrected speed. Let $\bar{W}_C = \{W^C_{ij}\}$ denote a vector of mass flow rate and $\overline{\mathrm{TR}}_C = \{\mathrm{TR}^C_{ij}\}$ denote a vector of temperature ratio at each pair of $\mathrm{PR}^C_i \in \overline{\mathrm{PR}}$ and $\mathrm{CN}^C_j \in \overline{\mathrm{CN}}$. A compressor map is represented as $\{\bar{W}_C, \overline{\mathrm{TR}}_C, \overline{\mathrm{CN}}_C, \overline{\mathrm{PR}}_C\}$.

Uncertainty in the compressor map is probabilistically represented using two independent nonstationary Gaussian processes. Probability distribution on a Gaussian process is given by a multivariate Gaussian distribution with mean and covariance function specified at each pair of $\{\mathrm{CN}^C_i, \mathrm{PR}^C_j\}$. Compressor map obtained from the first step, $\{(\bar{\mu}_{W_C}, \bar{\mu}_{\mathrm{TR}_C}, \overline{\mathrm{CN}}_C, \overline{\mathrm{PR}}_C)\}$ is used as a mean vector. Any real valued positive definite function can be used to define a covariance function. Steady-state response of a gas turbine engine is a function of local area of component maps. Hence, effect of addition of information at a point diminishes with increase in the Euclidean distance. This spread of information is given by correlation function. In the present work, exponentially decaying radial basis function is used as a correlation function. The covariance function is specified as

$$\mathrm{cov}(\mathrm{CN}_k, \mathrm{PR}_k, \mathrm{CN}_l, \mathrm{PR}_l) = \sigma_k\sigma_l \exp(-(\lambda_{\mathrm{PR}}(\mathrm{PR}_k-\mathrm{PR}_l)^2 + \lambda_{\mathrm{CN}}(\mathrm{CN}_k-\mathrm{CN}_l)^2)) \quad (15)$$

where correlation strength λ is assumed to be fixed and σ_k is a standard deviation in performance value for kth pair of corrected speed and pressure ratio. Thus, prior probability of a compressor map is given by

$$\Pr(\bar{W}_c, \overline{\mathrm{TR}}_c) \propto \exp\left(-\frac{1}{2}\times(\bar{W}_c-\bar{\mu}_{W_c})^T \times \Sigma^{-1}_{W_c} \times (\bar{W}_c-\bar{\mu}_{W_c})\right) \times \exp\left(-\frac{1}{2}\times(\overline{\mathrm{TR}}_c-\bar{\mu}_{\mathrm{TR}_c})^T \times \Sigma^{-1}_{\mathrm{TR}_c} \times (\overline{\mathrm{TR}}_c-\bar{\mu}_{\mathrm{TR}_c})\right) \quad (16)$$

where Σ is a covariance matrix obtained using Eq. (15). On specification of a compressor map, mass flow rate W^C at any corrected speed CN^C and pressure ratio PR^C are predicted as follows. Let μ_{W_C} and σ_{W_C} denote interpolated mean and standard deviation at $\{\mathrm{CN}^C, \mathrm{PR}^C\}$. Conditional on a given compressor mass flow rate map $\bar{W}_C$, probability distribution of W^C is normally distributed with mean μ and standard deviation σ that are given by Kalman filter equation as

$$\mu = \mu_{W_C} + r^T_{W_C}\Sigma^{-1}_W(\bar{W}_C-\bar{\mu}_{W_C}) \qquad \sigma^2 = \sigma^2_{W_C} - r^T_{W_C}\Sigma^{-1}_W r_{W_C} \quad (17)$$

where r_{W_C} is a vector of covariance between $\{\mathrm{CN}^C, \mathrm{PR}^C\}$ and each $\{\mathrm{CN}^C_i, \mathrm{PR}^C_j\}$. W^C is sampled from this normal distribution. TR^C is similarly sampled at any $\{\mathrm{CN}^C, \mathrm{PR}^C\}$.

Prior for Turbine Map

Similar to compressor map, turbine map is a specification of mass flow rate and enthalpy rise as a function of pressure ratio and corrected speed, represented here as $\{\bar{W}_T, \bar{H}_T, \overline{\mathrm{CN}}_T, \overline{\mathrm{PR}}_T\}$. Similar to the compressor map, uncertainty in turbine enthalpy rise map is represented using a nonstationary Gaussian process. During the majority of the operational envelope, turbine operates in the chocked condition that maintains constant corrected mass flow rate. Uncertainty in the turbine mass flow rate map is given by uncertainty in the choked corrected turbine mass flow rate, which is represented using a Gaussian distribution. Thus, prior uncertainty in the turbine map is probabilistically given by

$$\Pr(\bar{W}_T, \bar{H}_T) \propto \exp\left(-\frac{1}{2}\times(\bar{H}_T-\bar{\mu}_{H_T})^T \times \Sigma^{-1}_{H_T} \times (\bar{H}_T-\bar{\mu}_{H_T})\right) \times \exp\left(-\frac{(W_T-\mu_{W_T})^2}{2\sigma^2_{W_T}}\right) \quad (18)$$

Prior for Discrepancy Function

The model structure uncertainty is given by an additive random discrepancy function $\delta_j(\bar{x})$ which is probabilistically represented using a stationary Gaussian process with mean μ_{δ_j} and covariance matrix Σ_{δ_j}. In the present paper, following covariance function for the Gaussian process is used

$$\mathrm{cov}\,(\bar{x}_1, \bar{x}_2) = \sigma^2_{\delta_j} \exp\left(-\sum_{k=1}^{d}\lambda^k_{\delta_j}(x_{1k}-x_{2k})^2\right) \quad (19)$$

where $d = 2$ for the present single spool gas turbine engine. Probability of a discrepancy function $\delta_j(\bar{x})$ is given by a multivariate Gaussian distribution which is defined at finite locations where system response is experimentally observed. Thus, on specification of mean μ_δ, variance $\sigma^2_{\delta_j}$ and $\bar{\lambda}_{\delta_j} = \{\lambda^k_{\delta_j}; k = 1, d\}$, probability of $\bar{\delta}_j$ is given by

$$\Pr(\bar{\delta}_j|\mu_{\delta_j}, \sigma^2_{\delta_j}, \bar{\lambda}_{\delta_j}) \propto |\Sigma_{\delta_j}|^{-1} \exp\left(-\frac{1}{2}(\bar{\delta}_j - \mu_{\delta_j})^T \Sigma^{-1}_{\delta_j}(\bar{\delta}_j - \mu_{\delta_j})\right) \tag{20}$$

μ_{δ_j}, $\sigma^2_{\delta_j}$ and $\bar{\lambda}_{\delta_j}$ are treated as uncertain hyperparameters with specified prior. Let us define set of respective hyperparameters using earlier notations as $\bar{\mu}_\delta$, $\bar{\sigma}^2_\delta$ and $\bar{\lambda}_\delta$.

Joint prior for $\mu_{\delta_j}, \sigma^2_{\delta_j}$ is specified using inverse Gamma–Gaussian distribution, which is a conjugate prior for stationary Gaussian process with uncertain mean and variance. μ_{δ_j} defines expected bias in the simulator predictions. In the absence of a priory information about the fixed bias in the simulator predictions, prior mean of the inverse Gamma–Gaussian distribution is assumed to be zero. However, conjugate prior for λ is not available. λ in each direction is always greater than zero to ensure nonsingular covariance matrix. Also, near zero value of the correlation strength results in an ill-conditioned covariance matrix and hence should be considered with low probability. A random variable with Gamma distribution satisfies these conditions. Hence in the present work, gamma distribution is used as a prior for $\bar{\lambda}_\delta$. Thus

$$\Pr(\bar{\mu}_\delta, \bar{\sigma}^2_\delta, \bar{\lambda}_\delta) \propto \prod_{j=1}^{M}\left\{(\sigma^2_{\delta_j})^{-\frac{1}{2}} \exp\left(-\frac{\mu^2_{\delta_j}}{2\sigma^2_{\delta_j}}\right) \times \left(\frac{1}{\sigma^2_{\delta_j}}\right)^{(\alpha_{\delta_j}-1)} \times \exp\left(-\frac{\beta_{\sigma_{\delta_j}}}{\sigma^2_{\delta_j}}\right) \times \prod_{k=1}^{d}(\lambda^k_{\delta_j})^{(\alpha_{\lambda^k_{\delta_j}}-1)} \exp(-\beta_{\lambda^k_{\delta_j}}\lambda^k_{\delta_j})\right\} \tag{21}$$

Prior information about hyperparameters is given by specifying α and β parameters of the Gamma distribution. The joint distribution of $(\bar{\delta}_j, \bar{\mu}_{\delta_j}, \bar{\sigma}^2_{\delta_j}, \bar{\lambda}_{\delta_j})$ is given by Eqs. (20) and (21) and multiplicative property of conditional probability.

Posterior Distribution

Uncertainty in experimental observations is probabilistically modeled using uncorrelated zero-mean multivariate Gaussian distribution with covariance matrix given by $\Sigma_{Y_{e_j}} = \sigma^2_{y_{e_j}} I_N$. Here, $\sigma^2_{y_{e_j}}$ is variance of experimental observation of jth system response and I_N is an $N \times N$ identity matrix. Thus, using Eq. (3), likelihood is given by

$$\Pr(\bar{Y}_e|\bar{\eta}_t, \bar{\delta}) \propto \prod_{j=1}^{M} \exp\left(-\frac{1}{2}(\bar{Y}_{e_j} - \bar{d}_j)^T \Sigma^{-1}_{Y_{e_j}}(\bar{Y}_{e_j} - \bar{d}_j)\right) \tag{22}$$

Prior for component maps is given by Eqs. (16) and (18) while prior for discrepancy function is given by Eq. (20). However, prior for discrepancy function depends on specification of hyperparameters that are uncertain. Prior for hyperparameters is given by Eq. (21). Using Bayes theorem, likelihood given by Eq. (22), prior for component maps, discrepancy function and its hyperparameters, and marginalization of $\bar{\delta}$, posterior distribution is given by

$$\begin{aligned} f(\bar{\eta}_t, \bar{\mu}_\delta, \bar{\sigma}^2_\delta, \bar{\lambda}_\delta) \propto{}& \prod_{j=1}^{M} |\Sigma_j|^{-\frac{1}{2}} \exp\left(-\frac{1}{2}(\bar{Y}_{e_j} - \bar{\mu}_j)^T \Sigma^{-1}_j (\bar{Y}_{e_j} - \bar{\mu}_j)\right) \\ &\times (\sigma^2_{\delta_j})^{-\frac{1}{2}} \exp\left(-\frac{\mu^2_{\delta_j}}{2\sigma^2_{\delta_j}}\right) \times \left(\frac{1}{\sigma^2_{\delta_j}}\right)^{(\alpha_{\sigma_j}-1)} \exp\left(-\frac{\beta_{\sigma_j}}{\sigma^2_{\delta_j}}\right) \\ &\times \prod_{k=1}^{d}(\lambda^k_{\delta_j})^{(\alpha_{\lambda^k_{\delta_j}}-1)} \exp(-\beta_{\lambda^k_{\delta_j}}\lambda^k_{\delta_j}) \times \exp\left(-\frac{1}{2} \times (\bar{W}_c - \bar{\mu}_{W_c})^T \right. \\ &\left. \times \Sigma^{-1}_{W_c} \times (\bar{W}_c - \bar{\mu}_{W_c})\right) \times \exp\left(-\frac{1}{2} \times (\overline{\mathrm{TR}}_c - \bar{\mu}_{\mathrm{TR}_c})^T \right. \\ &\left. \times \Sigma^{-1}_{\mathrm{TR}_c} \times (\overline{\mathrm{TR}}_c - \bar{\mu}_{\mathrm{TR}_c})\right) \end{aligned} \tag{23}$$

where

$$\Sigma_j = \Sigma_{Y_{e_j}} + \Sigma_{\delta_j} \qquad \bar{\mu}_j = \{T(\bar{x}_i, \bar{\eta}_t) + \mu_{\delta_j}\}; \qquad i = 1, \ldots, N \tag{24}$$

Expert Judgment

A typical speed line on a compressor map represents the relation between pressure ratio and mass flow rate. At the highest pressure ratio, mass flow rate is low and increases gradually with decreasing pressure ratio and becomes constant at chocking conditions. Denote this expert information by I_2, which can be used along with experimental observations for the Bayesian calibration. To add information I_2, it is necessary to convert this information into the probabilistic data. Probabilistic expert information is supplied to the framework as follows (see Fig. 2). After Bayesian update using experimental observations, mean compressor map may not be acceptable to an expert due to its shape. Probabilistic expert information is provided in terms of performance values in the compressor map, denoted as pseudodata in the figure. These pseudodata are generated at all pressure ratios below updated point a by assuming linear change in slope of a speed line with the maximum slope at surge line and zero slope near chocking. After addition of the expert information, acceptable shape of the mean map is obtained. Further expert information for any map can similarly be incorporated.

Let $\bar{W}_e$ denote the vector of mass flow rate according to an expert opinion, with associated vector of standard deviation $\bar{\sigma}_e$. Let $\bar{\mu}_w$ is posterior mean of compressor mass flow rate map after addition of information using experimental observation. Posterior probability of a compressor mass flow rate map after addition of expert opinion is given by

$$f(\bar{W}|\bar{W}_e) \propto \exp\left(-\frac{1}{2}(\bar{W}_e - \bar{W})^T \Sigma^{-1}_e (\bar{W}_e - \bar{W})\right) \times \exp\left(-\frac{1}{2}(\bar{W} - \bar{\mu}_W)^T \Sigma^{-1}_w (\bar{W} - \bar{\mu}_W)\right) \tag{25}$$

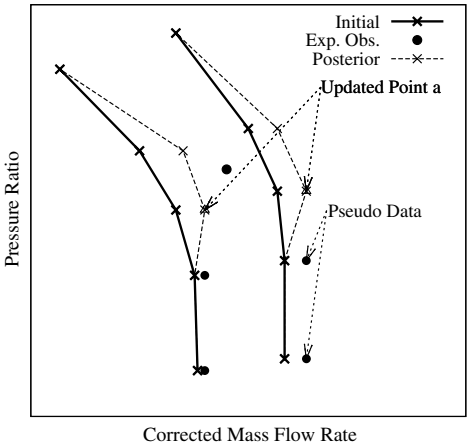

Fig. 2 Bayesian update using expert opinion.

Table 2 Engine design point performance data

Variable	Unit	Values
Corrected mass flow rate	kg.sec^{-1}	21.0
Compressor pressure ratio	——	6.00
Compressor temperature ratio	——	1.81
Spool speed	rpm	12700
Corrected fuel flow	kg.sec^{-1}	0.27
Combustor exit temperature	K	1100

where Σ_e is a diagonal matrix with diagonal elements given by $\bar{\sigma}_e$. Equation (25) can further be simplified as

$$f(\bar{W}|\bar{W}_e) \propto |\Sigma_{nw}|^{-1/2} \exp\left(-\frac{1}{2}(\bar{W}-\bar{\mu}_{nw})^T \Sigma_{nw}^{-1}(\bar{W}-\bar{\mu}_{nw})\right) \tag{26}$$

where

$$\Sigma_{nw} = (\Sigma_e^{-1} + \Sigma_w^{-1})^{-1} \qquad \mu_{nw} = \Sigma_{nw}^{-1}(\Sigma_w \mu_w + \Sigma_e W_e) \tag{27}$$

Uncertainty Propagation

The Monte–Carlo method is used to propagate posterior uncertainty in $\{\bar{\eta}_t, \bar{\mu}_\delta, \bar{\sigma}_\delta^2, \bar{\lambda}_\delta\}$ to simulator predictions. A large finite set of samples from posterior distribution of $\{\bar{\eta}_t, \bar{\mu}_\delta, \bar{\sigma}_\delta^2, \bar{\lambda}_\delta\}$ is collected. System response is predicted for each sample of $\bar{\eta}_t$. Conditional on a sample of $\{\bar{\mu}_\delta, \bar{\sigma}_\delta^2, \bar{\lambda}_\delta\}$, probability distribution of discrepancy function is defined. A sample of $\bar{\delta}$ is drawn from this probability distribution. However, $\bar{\delta}$ defines discrepancy at control input settings where system responses are experimentally observed. At other control input settings, discrepancy is a normally distributed random variable with mean and standard deviation given by Kalman filter equations [see Eq. (17)]. Value of discrepancy is sampled from this normal distribution. Mean and standard deviation of the *true* system response can be calculated using samples of predicted system response and associated discrepancy. In the present paper, Bayesian confidence bound on predicted system response is calculated using mean and standard deviation of *true* system response.

Details of Implementation

For complex simulator models, analytical solution of Eq. (23) is not available. In the present paper, authors use Markov Chain Monte–Carlo (MCMC) method to sample from the posterior distribution. One of the most popular and simplest MCMC algorithm is the Metropolis algorithm [25]. Metropolis algorithm starts at some point $\bar{\theta}_0$ and generates random samples by repeating following steps, supposing present state is $\bar{\theta}_i$:

1) Select a new trial point $\bar{\theta}_*$ using symmetric proposal distribution $f(\bar{\theta}_*|\bar{\theta}_i)$.

2) Calculate the acceptance probability

$$A(\bar{\theta}_*, \bar{\theta}_i) = \min\left[1, \frac{\Pr(\bar{\theta}_*)}{\Pr(\bar{\theta}_i)}\right] \tag{28}$$

3) Accept $\bar{\theta}_*$ with probability $A(\bar{\theta}_*, \bar{\theta}_i)$.

4) If trial point is accepted, then $\bar{\theta}_{i+1} = \bar{\theta}_*$ else $\bar{\theta}_{i+1} = \bar{\theta}_i$.

To ensure convergence of the chain, a predefined number of initial samples are rejected and sampling is started after this initial burnout period. Acceptance rate of around 30% provide sufficient sampling from the target stationary distribution [26]. The collected posterior samples are used to propagate the uncertainty to simulator predictions using Monte–Carlo method.

The first step is not computationally intensive and is easily implemented on a personal desktop. Markov Chain is initiated from prior mean. Zero-mean Gaussian distribution is used as a proposal distribution. However, step two is computationally expensive and requires a high-performance parallel computer for implementation. Step two of the Bayesian framework is implemented on a parallel computer using message passing interface. Independent Markov Chains are initiated from different starting points on each processor of the computer. Zero-mean multivariate Gaussian distributions with covariance matrix same as that of the prior are used as proposal distribution for component maps represented using Gaussian processes. For other parameters, zero-mean Gaussian process is used as a proposal distribution. Samples are collected after predefined initial burnout period for each Markov Chain. Authors have investigated other proposal distributions also, however, found the present distribution optimal in terms of convergence. However, satisfactory acceptance rate is not obtained for Markov Chain started from a low prior probability region. Hence, care should be taken to avoid low prior probability region for initiation of a Markov Chain.

Results and Discussion

The proposed Bayesian framework is demonstrated for core of a design intent twin-spool turbofan engine. The design intent engine is a low-bypass, twin-spool, mixed flow turbofan engine. The core engine is a single spool turbojet engine with six-stage axial flow compressor driven by a single stage turbine. From the total air mass flow through the engine, fixed percentage is extracted as a bleed from intermediate compressor stage and exit of the compressor. The bleed from an intermediate compressor stage is used for cooling the turbine rotor while bleed from the compressor exit is used for cooling the nozzle guide vanes and the rotor. Some power is extracted from the spool for driving the accessories. Turbine exit mass flow is expanded in a convergent nozzle. Table 2 shows design performance data provided by the engine manufacturer at the International Standard Atmosphere sea level static conditions.

Manufacturer has tested the core engine separately from the turbofan engine. Core is tested at an altitude test facility to experimentally observe steady-state and transient system responses.

Table 3 Engine test data

	All values normalized as explained above							
	Atmospheric pressure, kPa	Atmospheric temperature, K	Fuel flow	Nozzle area	Compressor exit total pressure	Spool speed	Jet pipe total pressure	Jet pipe total temperature
	Set one (for calibration)							
1	91.1	300.38	1.00	0.00	1.00	1.00	1.00	1.00
2	91.1	300.38	0.64	0.18	0.92	0.98	0.91	0.91
3	91.1	300.38	0.35	0.42	0.83	0.96	0.83	0.84
4	91.1	300.38	0.00	1.00	0.71	0.93	0.72	0.75
5	91.1	300.38	0.06	0.20	0.65	0.89	0.80	0.79
	Set two (for comparison)							
1	89.9	298.8	0.33	0.01	0.74	0.92	0.88	0.87
2	89.9	298.8	0.49	0.01	0.82	0.94	0.92	0.90
3	89.9	298.8	0.78	0.01	0.93	0.97	0.98	0.96
4	89.9	298.8	1.07	0.01	1.01	0.99	1.04	1.02

Table 4 Details of Bayesian analysis (step one)

Initial information		
Parameter	Mean	Standard deviation
Scaling compressor mass flow (W_c)	3.53	1.15
Scaling compressor temperature ratio (TR_c)	1.86	0.03
Scaling turbine mass flow (W_T)	1.01086	0.35
Scaling turbine enthalpy (ΔH_T)	279.63	95.0
After Bayesian update		
Scaling compressor mass flow (W_c)	3.46	0.11
Scaling compressor temperature ratio (TR_c)	1.91	0.007
Scaling turbine mass flow (W_T)	1.018	0.03
Scaling turbine enthalpy (ΔH_T)	286.77	4.625

Engine transients are performed by giving ramp input to fuel flow and nozzle throat area. Steady states are observed by maintaining constant fuel flow and nozzle throat area for long duration of time. The engine manufacturer provided nine steady states with intermediate transients, however, did not provide information about experimental uncertainties. Compressor exit total pressure P_3, jet pipe total pressure P_j, jet pipe total temperature T_j, and spool speed N are used as system responses. Details of steady states are given in Table 3. It may be noted that due to proprietary nature of the data, all the system responses are given as percentages of their highest values, whereas, control inputs are normalized in 0–1 range. Steady states are classified in two sets. Set one includes five steady-state points which are used for Bayesian calibration. A total of four steady-state points are included in set two, which along with intermediate transients are used for comparison with predicted system response of calibrated simulator.

For the step one, first data point given in Table 3, set one is used. The methodology is initiated from arbitrary base component maps with high uncertainty, which approximates complete lack of knowledge. Fixed standard deviation is used to represent model uncertainty which prevent overcalibration of component maps. Markov Chain is started from scaling parameters of the base maps. A total of 100,000 samples are collected after initial burnout period of 10,000 samples. Step one of the Bayesian framework results in the global update of the component maps. It may be noted that the step one is devised to provide initial component maps for step two in view of complete lack of knowledge. However, present industrial practices ensure availability of component maps with some confidence. In such scenario, step one may not be required and the framework may be initiated from the step two.

Table 4 give details of the Bayesian calibration after step one. Significant change in the probability distribution of the scaling parameters is observed, with update in standard deviation especially noticeable. Large change in the standard deviation signifies availability of considerable information in likelihood as compared with the prior. Ratio of prior to posterior standard deviation is maximum for scaling turbine enthalpy, while, minimum for scaling compressor temperature ratio.

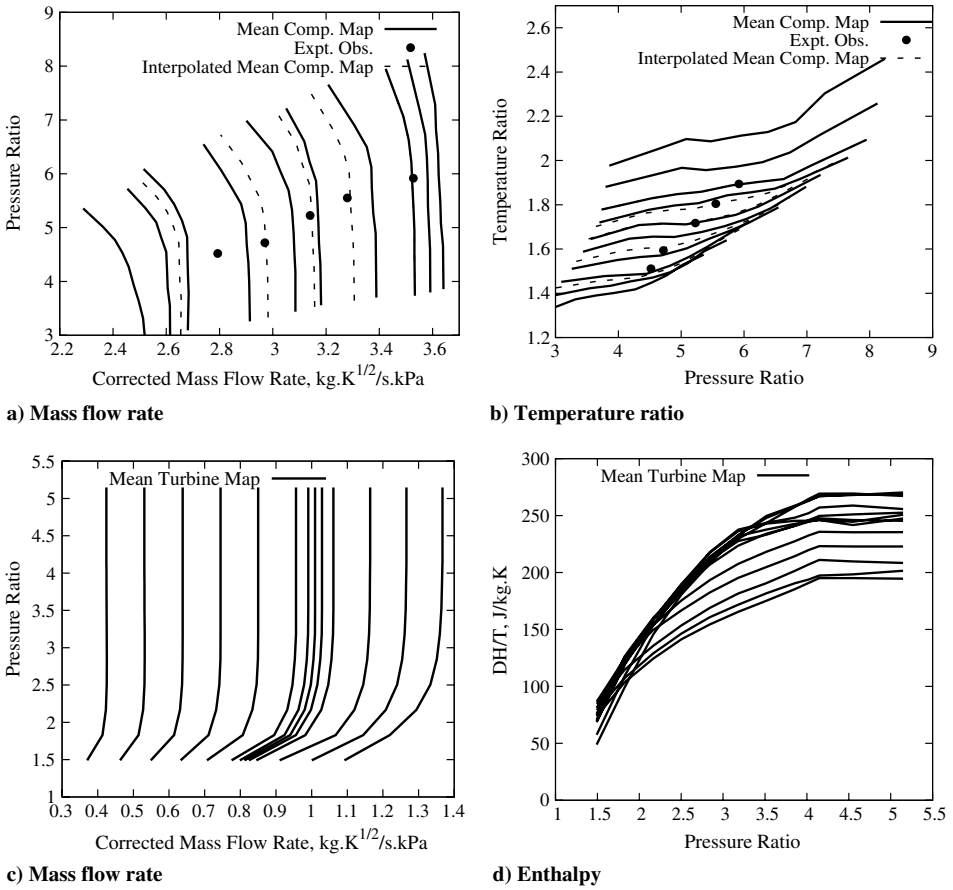

Fig. 3 Posterior mean maps after step two.

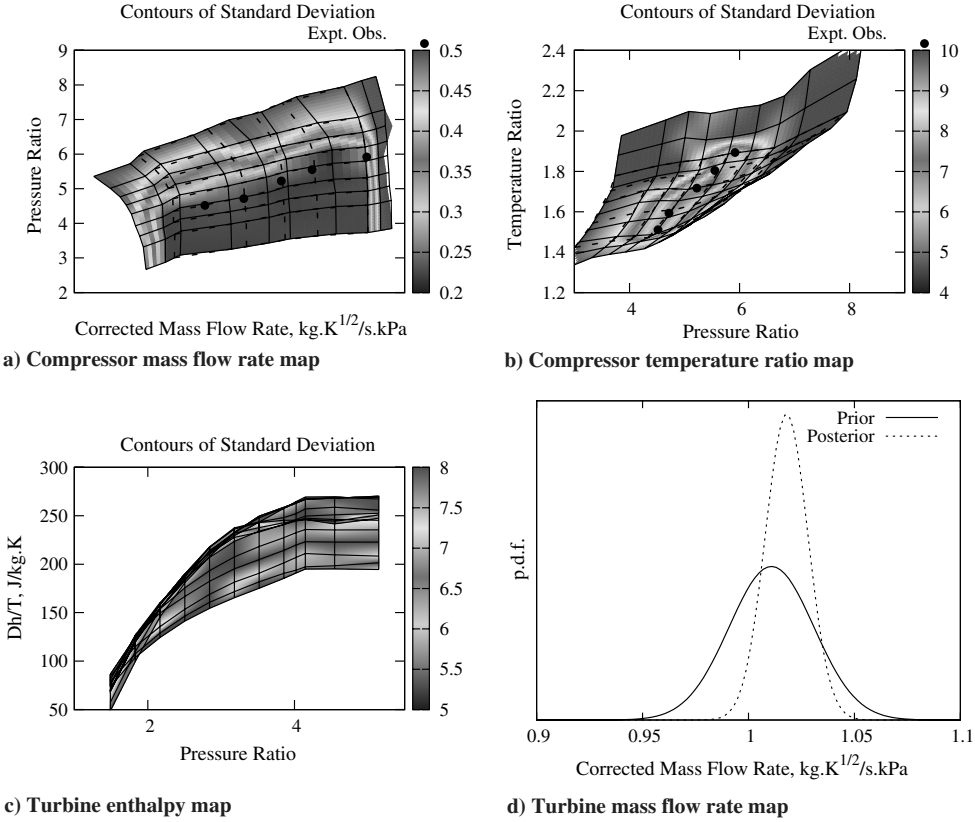

a) Compressor mass flow rate map **b) Compressor temperature ratio map**

c) Turbine enthalpy map **d) Turbine mass flow rate map**

Fig. 4 Contours of standard deviation.

For step two of the Bayesian framework, all the five steady-state points given in Table 3, set one are used. It may be noted that the first data point is used twice in the Bayesian framework. In step one, set of component maps is generated by a set of possible values of scaling parameters. In the second step, component maps are represented using Gaussian processes that define a set of all the real valued functions. Set of component maps in step one is a subset of set of component maps in step two. Thus, probability measure in step one and step two are different. Hence, first data point is used in step two also to update the prior probability.

Prior uncertainty in component maps is represented by independent nonstationary Gaussian processes with mean function given by posterior mean of the step one. Since no information is available to the contrary, constant standard deviation is specified at all points on the component maps. However, methodology can be implemented without change if varying standard deviation is specified. In the present work, constant standard deviation of 2.5% of the maximum performance value is used for all the Gaussian processes. For turbine mass flow rate, posterior mean, and standard deviation of step one are used to specify prior for step two. Prior for discrepancy function is given by zero-mean stationary Gaussian process. For all the system responses, prior for $\frac{1}{\sigma_\delta^2}$ is given by Gamma distribution $\Gamma(3.0, 0.2)$ while $\Gamma(1.2, 0.2)$ prior is used for both fuel flow and nozzle area. Five independent Markov chains with different starting points are used to sample from posterior distribution. A total of 500,000 samples are collected after burnout period of 10,000 samples for each Markov chain.

Figure 3 shows posterior mean maps after step two. Operating points of the experimental observations used for the Bayesian calibration are also shown on the compressor map. It may be noted that the experimental observations may not always fall on the available speed lines, and the map is interpolated at other operating points. These interpolated speed lines for the operating points of the experimental observations are also shown on the compressor map. Information about operating points on the turbine map was not available, and hence not shown in the figure. Update is observed in

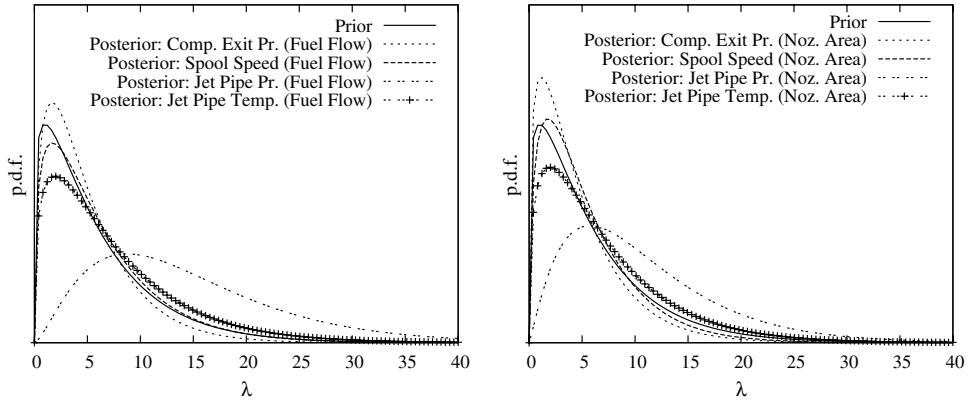

a) Fuel flow **b) Nozzle area**

Fig. 5 Probability distribution function of λ_δ.

Table 5 Statistics of posterior distribution λ_δ

	Fuel flow				Nozzle area			
	α	β	Mean	Mode	α	β	Mean	Mode
Prior	1.20	0.20	6.00	1.00	1.20	0.20	6.00	1.00
Compressor exit pressure	1.48	0.29	5.1	1.66	1.32	0.28	4.73	1.16
Spool speed	1.37	0.22	6.22	1.68	1.48	0.27	5.48	1.77
Jet pipe pressure	2.49	0.17	14.64	8.76	2.15	0.20	10.75	8.75
Jet pipe temperature	1.35	0.18	7.50	1.95	1.38	0.19	7.08	1.95

the vicinity of the experimental data for component maps represented using Gaussian processes (Figs. 3a–3c). Operating points are close to the interpolated compressor map for all but the last point. Though the experimental observations are independent, model uncertainty results in the correlated information. Because of the correlation, last point has less information for Bayesian calibration as compared with middle points. Hence update is not significant for the last experimental observation. Acceptable shape of the posterior mean compressor mass flow rate maps (Fig. 3a) is obtained by addition of information through expert opinion. However due to lack of expert information, update in posterior mean compressor temperature ratio map (Fig. 3b) and turbine enthalpy rise map (Fig. 3c) is localized near the region where experimental observations are added. Posterior mean turbine mass flow rate map, shown in Fig. 3d), is globally updated in step two also.

Figures 4a–4c show contours of standard deviation for component maps while Fig. 4d shows posterior distribution of turbine chocked corrected mass flow rate. From the figure, it may be noted that the standard deviation of all the component maps have reduced. Most significant reduction is observed for the compressor mass flow rate map. This is due to the fact that in addition to the experimental observations, expert opinion is also used as a source of information. Least spread in the information is observed for the turbine enthalpy map (Fig. 4c). For a given range of spool speed, turbine corrected rotational speed has a narrow range. Thus, experimental observations contain information about limited number of turbine corrected rotational speed lines. There is no significant change in the mean of prior and posterior distribution of the turbine chocked mass flow rate map. This is expected, since, the information available for Bayesian update in the step one and step two is same. However, standard deviation for the posterior is less than the prior, signifying the increased confidence in the map.

Figure 5 shows comparison of prior and posterior probability distribution of λ_δ. For compressor exit pressure, probability of the mode is higher than the prior for both fuel flow and nozzle area. Probability of mode of λ_δ for nozzle area is higher than the fuel flow. The posterior probability indicates increased confidence of value of λ_δ near mode as compared with prior. For spool speed, posterior distribution of λ_δ is also close to prior for both fuel flow and nozzle area. However, probability of mode of λ_δ for fuel flow is lower than the prior while for nozzle area it is higher than the prior. Posterior

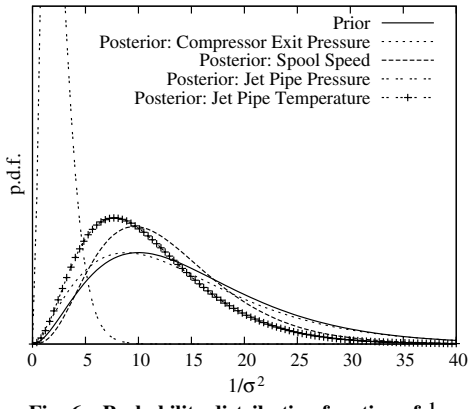

Fig. 6 Probability distribution function of $\frac{1}{\sigma_\delta^2}$.

Table 6 Statistics of posterior distribution $(\frac{1}{\sigma_\delta^2})$

	α	β	Mean	Mode
Prior	3.00	0.20	15.0	10.0
Compressor exit pressure	2.59	0.18	14.4	8.83
Spool speed	3.99	0.31	12.87	9.65
Jet pipe pressure	3.16	1.32	2.38	1.63
Jet pipe temperature	3.23	0.29	11.13	7.69

distribution of λ_δ deviates from prior with lower probability of mode for both fuel flow and nozzle area in case of jet pipe pressure and jet pipe temperature. The deviation is significant for λ_δ of jet pipe pressure with mode moving towards higher value. Important statistics of prior and posterior distribution for λ_δ is given in Table 5. Change in the value of β from prior to posterior is found to be insignificant for all the system responses, however, considerable update is observed in α for jet pipe pressure. Posterior mean and mode of λ_δ has increased significantly from prior for jet pipe pressure. Posterior indicates that the discrepancy between prediction and experimental observation of jet pipe pressure is expected to be poorly correlated of uncorrelated.

Comparison of prior and posterior probability distribution of $\frac{1}{\sigma_\delta^2}$ for all the system responses is shown in Fig. 6. The posterior distribution shows movement towards left, signifying increased uncertainty in the model as compared with the prior. Posterior distribution of $\frac{1}{\sigma_\delta^2}$ for discrepancy function of compressor exit pressure is close to prior, while in case of other system responses posterior deviates from the prior. Probability of the mode is higher than the prior for spool speed, jet pipe pressure and jet pipe temperature, indicating increased confidence on the value of $\frac{1}{\sigma_\delta^2}$ at mode. Significant change in the probability distribution of $\frac{1}{\sigma_\delta^2}$ for jet pipe pressure is observed, with posterior probability distribution moving significantly towards left. Important statistics of the posterior distribution is given in Table 6. Change in the value of α is found to be insignificant with maximum change observed for spool speed. However, value of β is updated considerably for jet pipe pressure. Value of posterior mean and mode has reduced for all the system responses, with significant change observed for jet pipe pressure. The table also give value of $\frac{1}{\sigma_\delta^2}$ at mean and mode for prior and all the system responses. From the table, it can be noted that posterior σ_δ for jet pipe pressure is considerably higher than the prior at both mean and mode, indicating significantly reduced confidence on the model for prediction of jet pipe pressure.

Statistics of posterior distribution of deviation functions suggest decrease in confidence on all the predictions as compared with the prior. The decrease is insignificant for prediction of compressor exit pressure, spool speed and jet pipe temperature. However, confidence on the posterior prediction of jet pipe pressure is significantly reduced. Posterior distribution of λ_δ for jet pipe pressure indicates poorly correlated discrepancy between model prediction and experimental observation. Since the uncertainty due to unknown or poorly known physics is expected to result in correlated discrepancy, uncorrelated discrepancy may be attributed to experimental observations. Thus, posterior distribution of λ_δ and $\frac{1}{\sigma_\delta^2}$ suggests requirement for verification and validation of the simulator model for jet pipe pressure predictions and a review of experimental observations of jet pipe pressure.

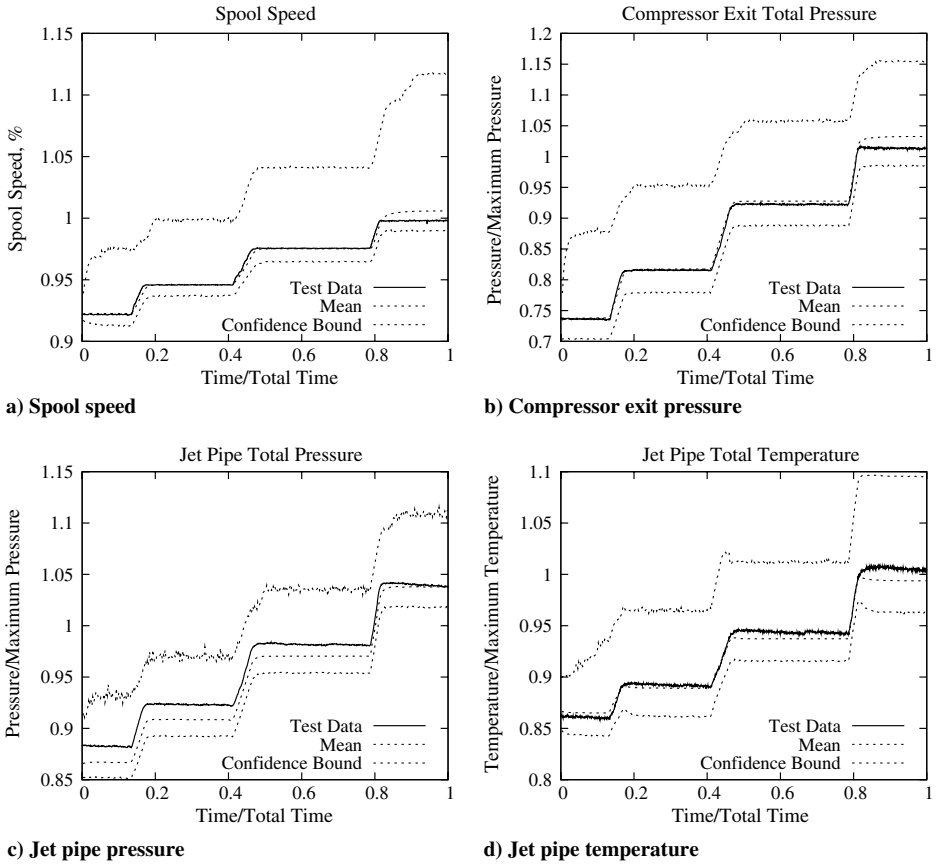

a) Spool speed **b) Compressor exit pressure**

c) Jet pipe pressure **d) Jet pipe temperature**

Fig. 7 Uncertainty propagation.

Posterior uncertainty in component maps and model structure is propagated to prediction of steady-state and transient system response. Four experimentally observed steady-state points provided by engine manufacturer (Table 3, set two) are used for comparison with simulator predictions. Transient performed using linear ramp change in control inputs with initial and final steady states given in Table 3, set two are also compared with simulated system response. Comparison is shown in Fig. 7. Ninety percent confidence bound on predictions is also shown. Close match is observed between test data and mean prediction of compressor exit pressure, spool speed, and jet pipe temperature. However, for jet pipe pressure, match is poor for lower values. Asymmetry in the confidence bounds indicates non-Gaussian nature of the propagated uncertainty, which is attributed to the nonlinearity in the simulator model. Since steady-state system response is used for the calibration that results in update of steady-state component maps. Time step for transients of interest are higher than the time step for dynamic behavior of component maps. Thus, steady-state component maps suffice for transient simulation of gas turbine engine. Hence, good match for transient performance is also observed after calibration using steady-state experimental observations.

Conclusions

Bayesian framework is a methodology for calibration of a computer simulator in presence of uncertainty in parameters and model. The framework also provides methodology to propagate the remaining uncertainty after calibration to system response. Use of independent Gaussian processes for probabilistic representation of deviation function allows prediction of discrepancy for each system response independently. This helps in identification of subsystem models that need to be verified and validated. Parameters α and β of the posterior distribution of $\frac{1}{\sigma_\delta^2}$ and λ_δ provide important guidelines about validity of the simulator model and experimental observations. Typically, $\alpha \approx 1$ and $\beta > \alpha$ for posterior distribution of $\frac{1}{\sigma_\delta^2}$ low confidence on the calibrated simulator. For this case, $\alpha < 1$ or $\beta > \alpha$ for posterior distribution of λ_δ indicates requirement for verification and validation of simulator model, whereas $\alpha > 1$ or $\beta \ll \alpha$ for posterior distribution of λ_δ specifies need for review of experimental observations.

Efficacy of Bayesian framework is demonstrated for calibration of a single spool turbojet engine simulator. The framework is used to infer compressor and turbine maps. Based on parameters of posterior distributions for $\frac{1}{\sigma_\delta^2}$ and λ_δ, calibrated simulator is found to be acceptable. However, verification and validation of the simulator model with focus on routines used for prediction of jet pipe pressure and a review of experimental observations of jet pipe pressure is advised. Calibrated simulator has predicted mean transient and steady-state system response that match closely with the experimental observations. Although demonstrated for a single spool engine simulator, the framework can be used for twin-spool engine simulator also without any change in the methodology. The framework can similarly be applied for other component maps and parameters. The framework can also be used for calibration of awkward component maps, however, prior maps should be used with very high uncertainty in second step and strong information through expert opinion.

Certain choices of priors made during present work can further be investigated. As already identified, gamma distribution is not a conjugate prior for correlation strength. In future, effect of choice of different probability distribution as a prior for correlation strength may be investigated. In the present work zero-mean stationary Gaussian process prior is used for discrepancy function. This particular choice of prior helps in providing useful information about veracity and validity of the simulator. However, if the framework is intended to be used only for calibration, nonstationary Gaussian process priors for discrepancy functions may prove to be more appropriate. In future, such a choice for the prior may be investigated.

At present, discrepancy functions for different system responses are modeled using independent Gaussian processes. Effect of correlated discrepancy functions on the calibration needs further investigation.

Acknowledgments

The research presented in this paper is carried out using the grant provided by Aeronautical Research and Development Board, India (project no. 08ARDB005). Authors express their gratitude toward Gas Turbine Research Establishment for providing engine test bed data.

References

[1] Oreskes, N., Shrader-Frechett, K., and Belitz, K., "Verification, Validation and Confirmation of Numerical Models in Earth Sciences," *Science*, Vol. 263, No. 5147, 1994, pp. 641–647. doi:10.1126/science.263.5147.641

[2] Moffat, R. J., "Describing the Uncertainties in Experimental Results," *Experimental Thermal and Fluid Science*, Vol. 1, No. 1, 1988, pp. 3–17. doi:10.1016/0894-1777(88)90043-X

[3] O'Hagan, A., "Eliciting Expert Beliefs in Substantial Practical Applications," *Journal of the Royal Statistical Society: Series D (The Statistician)*, Vol. 47, No. 1, 1998, pp. 21–35. doi:10.1111/1467-9884.00114

[4] Mehta, U. B., "Some Aspects of Uncertainty in Computational Fluid Dynamics Results," *Journal of Fluids Engineering*, Vol. 113, No. 4, 1991, pp. 538–543. doi:10.1115/1.2926512

[5] Mehta, U. B., "Guide to Credible Computer Simulations of Fluid Flows," *Journal of Propulsion and Power*, Vol. 12, No. 5, 1996, pp. 940–948. doi:10.2514/3.24126

[6] Oberkampf, W. L., DeLand, S. M., Rutherford, B. M., Diegert, K. V., and Alvin, K. F., "Error and uncertainty in modeling and simulation," *Reliability Engineering and System Safety*, Vol. 75, No. 3, 2002, pp. 335–357.

[7] O'Hagan, A., and Oakley, J. E., "Probability is Perfect, but We Can't Elicit it Perfectly," *Reliability Engineering and System Safety*, Vol. 85, Nos. 1–3, 2004, pp. 239–248.

[8] Helton, J. C., and Oberkampf, W. L., "Alternative Representations of Epistemic Uncertainty," *Reliability Engineering and System Safety*, Vol. 85, Nos. 1–3, 2004, pp. 1–10.

[9] de Finetti, B., *Theory of Probability*, Vol. 1, Wiley, New York, 1971.

[10] Bernardo, J. M., and Smith, A. F. M., *Bayesian Theory*, Wiley, New York, 1994.

[11] Robert, C. P., *The Bayesian Choice*, Springer, New York, 2007.

[12] Glimm, J., and Sharp, D. H., "Prediction and the Quantification of Uncertainty," *Physica D*, Vol. 133, Nos. 1–4, 1999, pp. 152–170. doi:10.1016/S0167-2789(99)00103-7

[13] Kennedy, M. C., and O'Hagan, A., "Bayesian Calibration of Computer Models," *Journal of the Royal Statistical Society: Series B (Statistical Methodology)*, Vol. 63, No. 3, 2001, pp. 425–464. doi:10.1111/1467-9868.00294

[14] Higdon, D., Kennedy, M., Cavendish, J. C., Cafeo, J. A., and Ryne, R. D., "Combining Field Data and Computer Simulations for Calibration and Prediction," *SIAM Journal of Scientific Computing*, Vol. 26, No. 2, 2005, pp. 448–446.

[15] Goldstein, M., and Rougier, J., "Probabilistic Formulations for Transferring Inferences fromMathematical Models to Physical Systems," *SIAM Journal of Scientific Computing*, Vol. 26, No. 2, 2005, pp. 467–487.

[16] Paulo, R., Sacks, J., Cafeo J. A., Cavendish, J., Lin, C. H., Bayarri, M. J., Berger, J. O., and Tu, J., "A Framework for Validation of Computer Models," *Technometrics*, Vol. 49, No. 2, 2007, pp. 138–153. doi:10.1198/004017007000000092

[17] Trucano, T. G., Swiler, L. P., Igusa, T., Oberkampf, W. L., and Pilch, M., "Calibration, Validation, and Sensitivity Analysis: What's What," *Reliability Engineering and System Safety*, Vol. 91, Nos. 10–11, 2006, pp. 1331–1357.

[18] Kelly, D. L., and Smith, C. L., "Bayesian Inference in Probabilistic Risk Assessment: The Current State of the Art," *Reliability Engineering and System Safety*, Vol. 94, No. 2, 2009, pp. 628–643.

[19] Roth, B., Doel, D., Mavris, D., and Beeson, D., "High Accuracy Matching of Engine Performance Models to Test Data," in *Proceedings of ASME Turbo Expo 2003*, American Society of Mechanical Engineers, Fairfield, NJ, 2003, pp. 129–137.

[20] Roth, B., Mavris, D., and Doel, D., "Estimation of Turbofan Engine Performance Model Accuracy and Confidence Bounds," *Proceedings of International Symposium on Air Breathing Engines 2003*, AIAA, Reston, VA, 2003.

[21] Doel, D., Roth, B., and Cissell, J., "Probabilistic Matching of Turbofan Engine Performance Models to Test Data," *Proceedings of ASME Turbo Expo 2005*, American Society of Mechanical Engineers, Fairfield, NJ, 2005, pp. 541–548.

[22] Tagade, P., Sudhakar, K., and Sane, S. K., "Bayesian Framework for Calibration of Gas Turbine Simulator," *Journal of Propulsion and Power*, Vol. 25, No. 4, 2009, pp. 987–991. doi:10.2514/1.38215

[23] Fawke, A. J., and Saravanamuttoo, H. I. H., "Digital Computer Methods for Prediction of Gas Turbine Dynamic Response," Society of Automotive Engineers Paper 710550, 1973.

[24] Adler, R. J., and Taylor, J. E., *Random Fields and Geometry*, Springer, New York, 2007.

[25] Metropolis, N., Rosenbluth, A. W., Rosenbluth, M. N., Teller, A. H., and Teller, E., "Equation of State Calculations by Fast Computing Machines," *Journal of Chemical Physics*, Vol. 21, No. 6, 1953, pp. 1087–1092. doi:10.1063/1.1699114

[26] Neal, R. M., "Probabilistic Inference using Markov Chain Monte Carlo Methods," Univ. of Toronto, Tech. Rept. CRG-TR-93-1, Department of Computer Science, 1993.

C. Tan
Associate Editor